Electronic Supplementary Information

Photoisomerization-induced patterning of ion-pairing materials based on anionic azobenzene and its complex with fluorescent π-electronic system

Ryohei Yamakado,* Issei Kitamura, Mitsuo Hara, Shusaku Nagano, Takahiro Seki and Hiromitsu Maeda*

Department of Organic Materials Science, Graduate School of Organic Materials Science, Yamagata University, Yonezawa 992–8510, Japan, Department of Molecular and Macromolecular Chemistry, Graduate School of Engineering, Nagoya University, Nagoya 464–8603, Japan, Department of Chemistry, College of Science, Rikkyo University, Tokyo 171–8501, Japan and Department of Applied Chemistry, College of Life Sciences, Ritsumeikan University, Kusatsu 525–8577, Japan; E-mail: yamakado@yz.yamagata-u.ac.jp, maedahir@ph.ritsumei.ac.jp

Table of Contents

1. Synthetic procedures and spectroscopic data

General Procedures. Starting materials were purchased from FUJIFILM Wako Pure Chemical Co., Nacalai Tesque Inc., Kanto Chemical Co. and Sigma-Aldrich Co. and were used without further purification unless otherwise stated. NMR spectra used in the characterization of products were recorded on a JEOL JNM-ECZ600R/M1 600 MHz spectrometers. All NMR spectra were referenced to solvent.

Poly(4-vinyl-*N*-dodecylpyridinium bromide), Br$^-$-P4VP$^+$. Poly(4-vinylpyridine) (P4VP) (0.30 g) and 1-bromododecane (3.6 mL, 14.4 mmol) were added to $CHCl_3$ (9 mL), and the mixture was heated at 60 °C for 3 days. After that, the mixture was poured into cold *n*-hexane to obtain Br$^-$-P4VP$^+$ (0.85 g, 83%) as a white solid. ^{1}H NMR (600 MHz, $CDCl_3$, 20 °C): δ (ppm) 8.86 (2H, Ar-H), 8.29 (2H, Ar-H), 4.62 (2H, NCH_2), 2.05 (2H, CH_2CH_2), 1.55–1.04 (18H, $C_2H_4(CH_2)_9$), 0.87 (3H, $C_{11}H_{22}CH_3$).

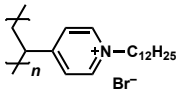

Poly(4-vinyl-*N*-dodecylpyridinium 4-(3,4,5-trihexadecylphenyl)diazenylbenzoate), Azb$^-$-P4VP$^+$. To a CH_2Cl_2 solution (3 mL) of Br$^-$-P4VP$^+$ (33.7 mg) was added potassium 4-(3,4,5-trihexadecylphenyl)-diazenylbenzoate) (**Azb**$^-$-K$^+$)[S1] (90.0 mg, 1 equiv for the repeating unit of Br$^-$-P4VP$^+$), and mixture was stirred at r.t. for 10 h. The resulting precipitate was removed by filtration, and the solvent was evaporated to afford **Azb**$^-$-P4VP$^+$ (98.2 mg, 88%) as an orange solid. ^{1}H NMR (600 MHz, $CDCl_3$, 20 °C): δ (ppm) 8.86 (2H, Ar-H (P4VP$^+$)), 8.29 (2H, Ar-H (P4VP$^+$)), 8.11 (2H, Ar-H (**Azb**$^-$)), 7.78 (2H, Ar-H (**Azb**$^-$)), 7.50 (2H, Ar-H (**Azb**$^-$)), 4.62 (2H, NCH_2), 2.59 (6H, ArCH_2 (**Azb**$^-$)), 1.83–0.67 (116H, $CH_2C_{11}H_{23}$ (P4VP$^+$) and $CH_2C_{15}H_{31}$ (**Azb**$^-$)).

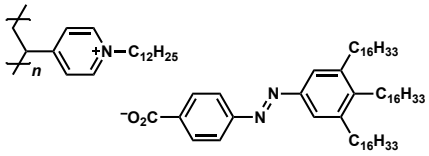

[S1] R. Yamakado, M. Hara, S. Nagano, T. Seki and H. Maeda, *Chem. Eur. J.*, 2017, **23**, 9244–9248.

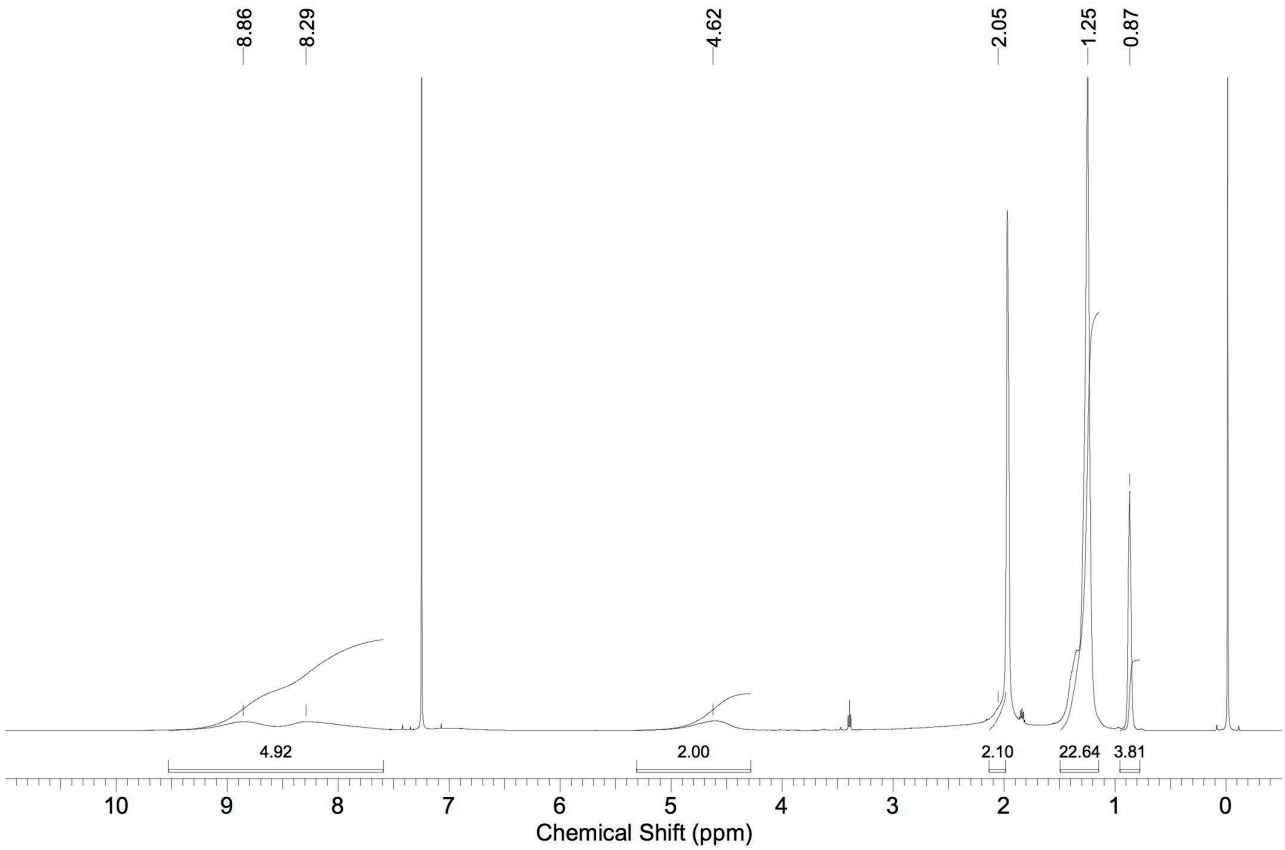

Fig. S1 ^{1}H NMR of Br^{-}-P4VP^{+} in $CDCl_3$.

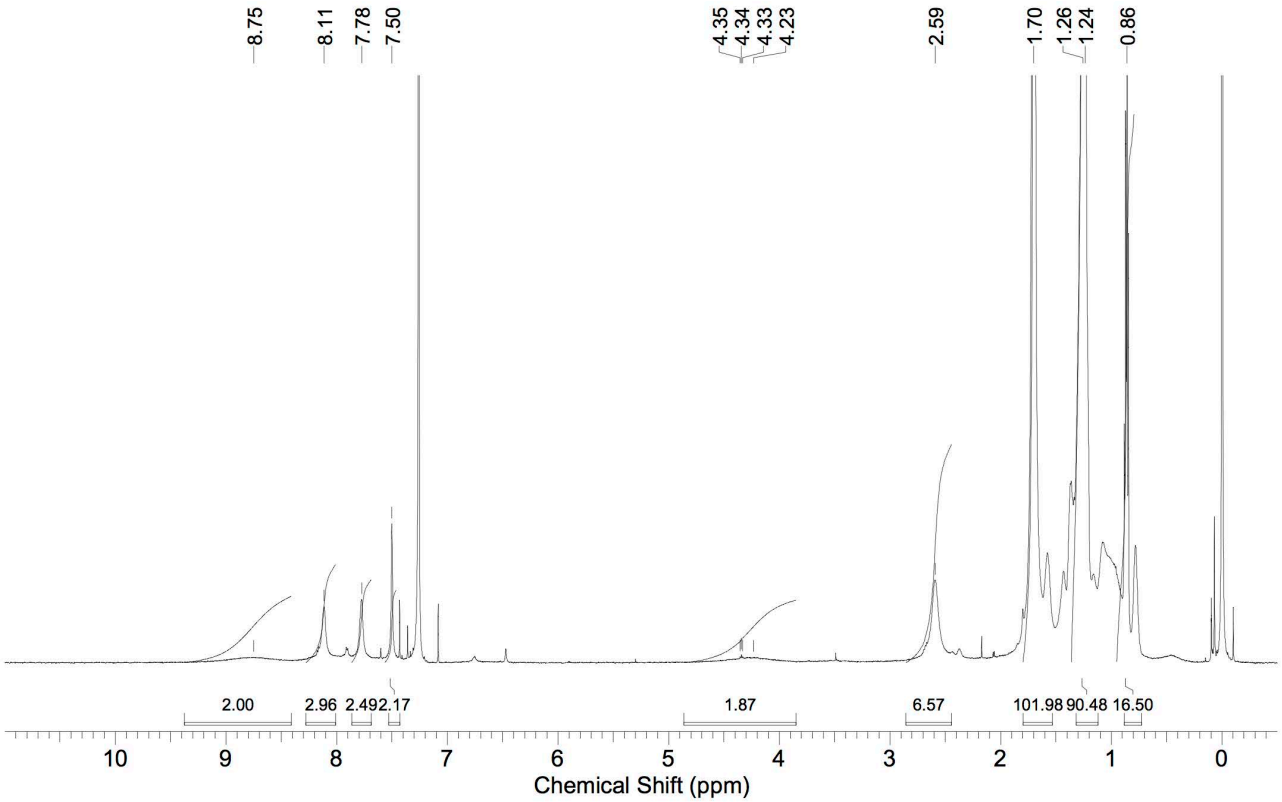

Fig. S2 ^{1}H NMR of **Azb**$^{-}$-P4VP^{+} in $CDCl_3$.

2. Thermal and photoisomerization properties

Differential scanning calorimetry (DSC). The phase transitions were measured on a differential scanning calorimetry (Hitachi SII EXSTAR DSC6220).

Preparation of sample films. Polymer thin films were prepared on a cleaned quartz substrate by spin-coating from a $CHCl_3$ solution (2 wt % and 1.5 wt% for **Azb**$^-$-P4VP$^+$ and **PB**·**Azb**$^-$-P4VP$^+$, respectively) at 2000 rpm for 30 s. The thickness of the films was estimated as ~200 nm by white-light interferometric microscopic topological images.

Photoirradiation. The UV (365 nm, 5 mW/cm^2) irradiation of the film sample was performed using Asahi-Spectra REX-250 super high-pressure mercury lamp with appropriate bandpass filters. All the irradiation times were set to 30 min, in which the surface topography was almost completed.

Absorption spectroscopy. UV-visible absorption spectra for films were measured by Ocean Optics QE6500 spectrometer/DH-2000-BAL light source system equipped with an Ocean Optics QR450-7-XSR reflection fiber probe. A mirror was placed at the bottom of a temperature-controlled stage (Mettler-Toledo FS-32/FP-90 system). The probing light passed the film samples and was reflected by the mirror. The UV (365 nm, 5 mW/cm^2) irradiation of the film sample was performed using Asahi-Spectra REX-250 super high-pressure mercury lamp with appropriate bandpass filters (Fig. S4).

Grazing-incidence small-angle X-ray scattering (GISAXS). GISAXS measurements were performed with a FR-E X-ray diffractometer equipped with R-AXIS IV two-dimensional (2D) detector (Rigaku Co.). Beam of 0.3 mm collimated Cu Kα radiation (λ = 0.154 nm) was used as an X-ray, and the camera length was set at 300 mm. Film samples were placed onto a pulse motor stage. An incident angle of the beam to the substrate surface was adjusted at ca. 0.18°−0.22° by using a Z pulse motor stage ALV-300-HM and an oblique pulse motor stage ATS-C310-EM (Chuo Precision Industrial Co., Ltd.). The X-ray irradiation time was set to 5 min, and the camera length was 300 mm. X-ray scattering patterns were recorded on an imaging plate (Fujifilm Co.). The temperature of the film sample was controlled using a ceramic heating system.

Contact angle measurement. Static water contact angles were characterized using a Contact Angle Meter CA-XP (Kyowa Interface Science Co., Ltd). The contact angle values were the average of five repeated measurements.

White-light interferometric microscopic (WLIM) topological images. The morphological changes were observed by WLIM (BE-S501, Nikon, Japan).

Microscope image. Optical and fluorescence microscope images were observed using Olympus BX51 equipped with a Nikon DS-Ri2 digital camera.

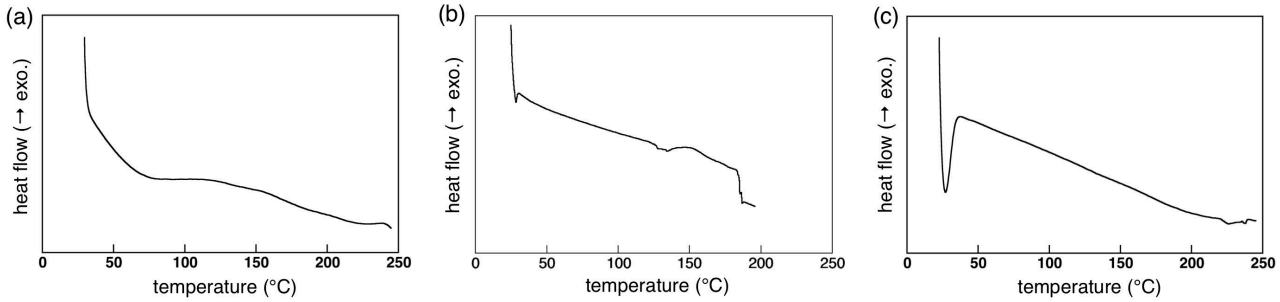

Fig. S3 DSC thermograms of (a) Br$^-$-P4VP$^+$, (b) **Azb**$^-$-P4VP$^+$, and (c) **PB**·**Azb**$^-$-P4VP$^+$ on heating at 5 °C/min.

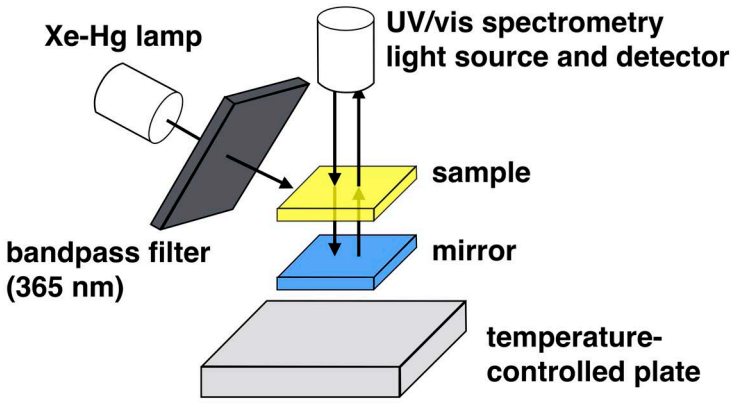

Fig. S4 Schematic illustration of a setup for observation of UV/vis absorption spectral changes under illumination at elevated temperatures.[S2]

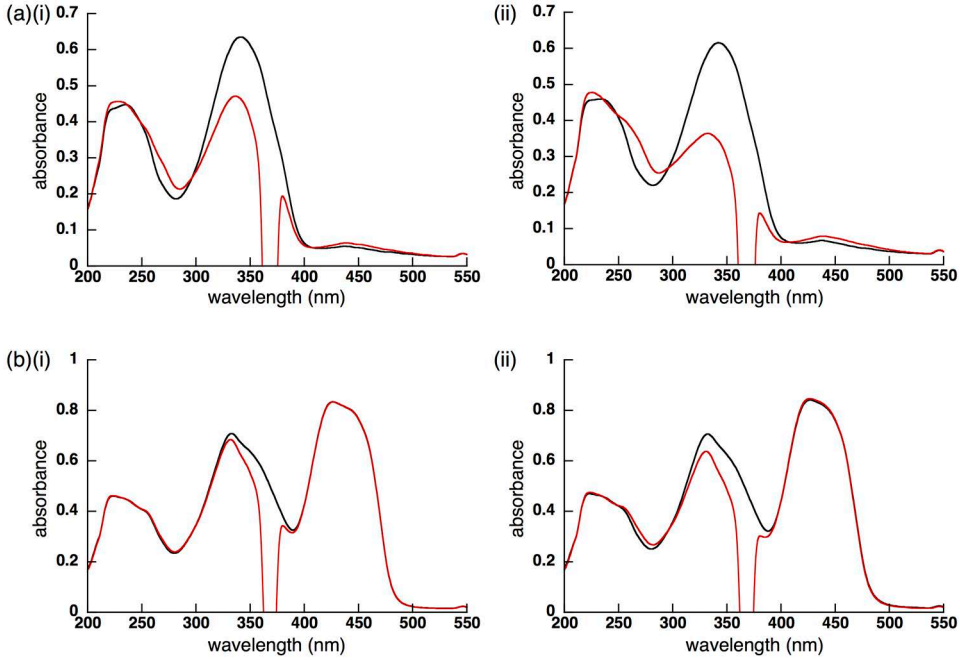

Fig. S5 UV/vis absorption spectral changes in spin-coated films: (a) **Azb**$^{-}$-P4VP^{+} at (i) 25 °C and (ii) 80 °C and (b) **PB**·**Azb**$^{-}$-P4VP^{+} at (i) 25 °C and (ii) 130 °C. Initial state (black) and photostationary state attained by excitation at 365 nm (red). Irradiation light (365 nm, 5 mW/cm^{2}) was also detected around 365 nm.

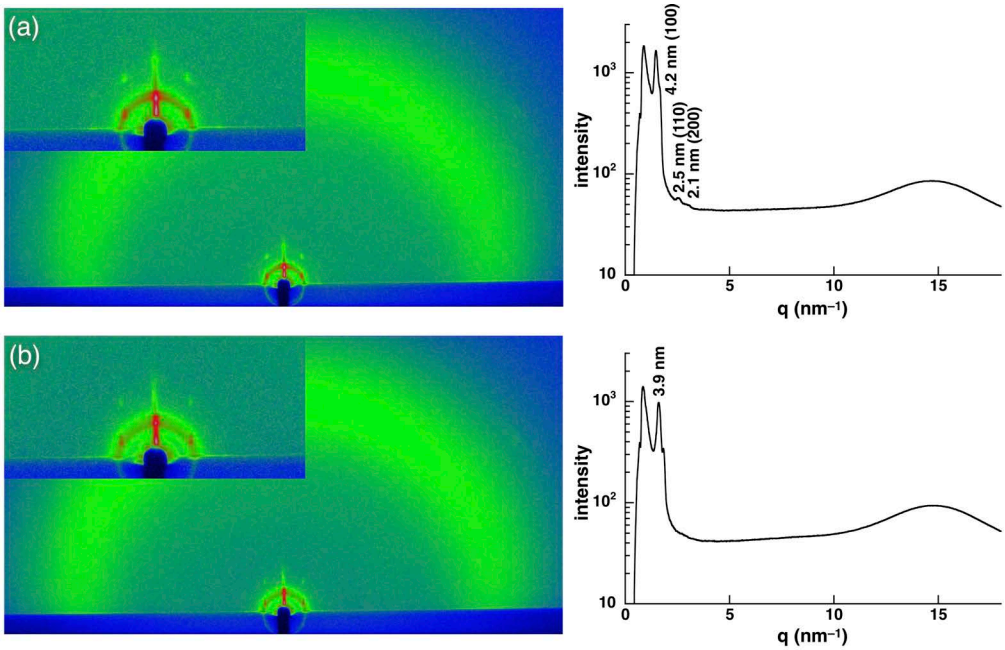

Fig. S6 GISAXS patterns (2D (left) and 1D (right) patterns) of **Azb**$^{-}$-P4VP^{+} at (a) 70 °C and (b) 70 °C with photoirradiation (365 nm, 5 mW/cm^2).

Table S1 GISAXS peaks of **Azb**$^{-}$-P4VP^{+} at 70 °C upon 1st heating. The peaks which can be indexed are represented.

	q (nm^{-1})	*d*-spacing (nm)	ratio	ratio (calc.)	*hkl*
Azb^{-}-P4VP^{+}	1.5	4.2	1.0	1.00	100
Col$_h$	2.5	2.5	0.60	0.58	110
a = 4.8 nm	3.0	2.1	0.50	0.50	200

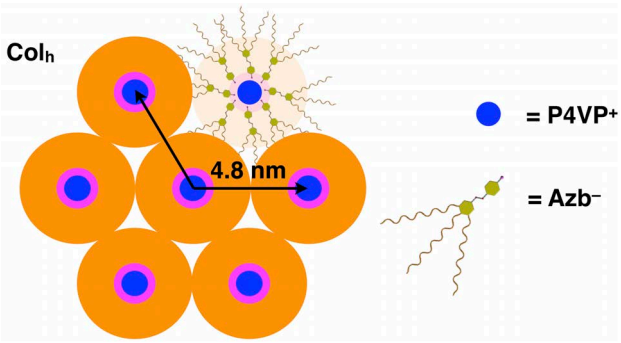

Fig. S7 Schematic illustration of the assembled arrangement in the hexagonal columnar (Col$_h$) structure of **Azb**$^{-}$-P4VP^{+} at 70 °C.

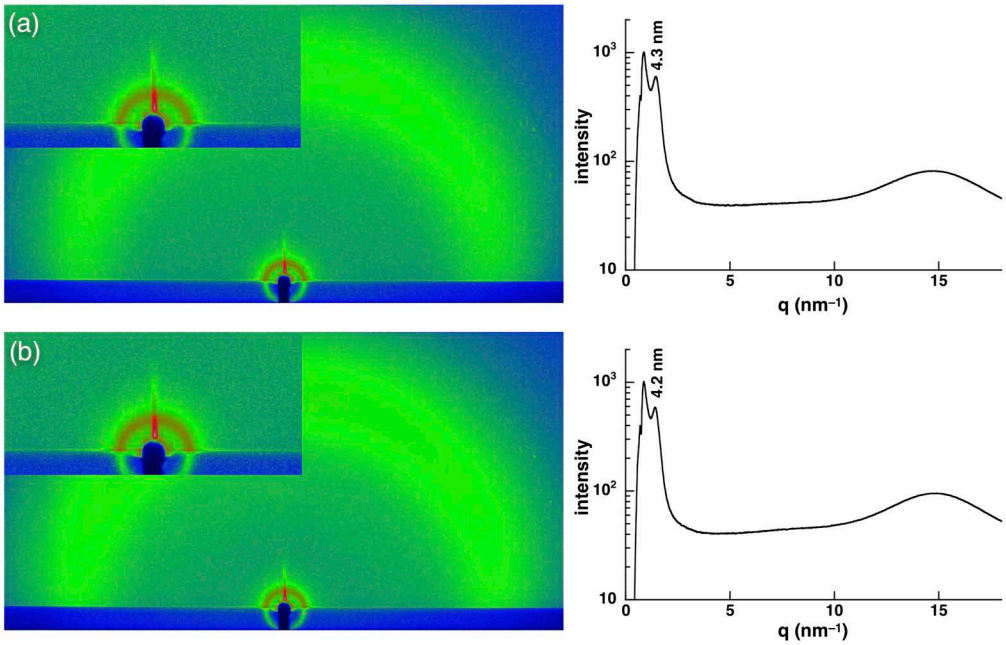

Fig. S8 GISAXS patterns (2D (left) and 1D (right) patterns) of **PB**·**Azb**$^{-}$-P4VP^{+} at (a) 90 °C and (b) 90 °C with photoirradiation (365 nm, 5 mW/cm^2).

Table S2 Contact angles of **Azb**$^{-}$-P4VP^{+}.

	Run 1	Run 2	Run 3	Run 4	Run 5	Average
After anneal	122.7°	122.2°	120.6°	121.2°	121.9°	121.7 ± 1.1°
After UV irradiation	117.6°	117.1°	117.4°	117.5°	117.4°	117.4 ± 0.3°

Table S3 Contact angles of **PB**·**Azb**$^{-}$-P4VP^{+}.

	Run 1	Run 2	Run 3	Run 4	Run 5	Average
After anneal	92.0°	92.7°	93.3°	93.0°	92.8°	92.8 ± 0.8°
After UV irradiation	87.4°	87.8°	87.2°	86.6°	88.5°	87.5 ± 1.0°

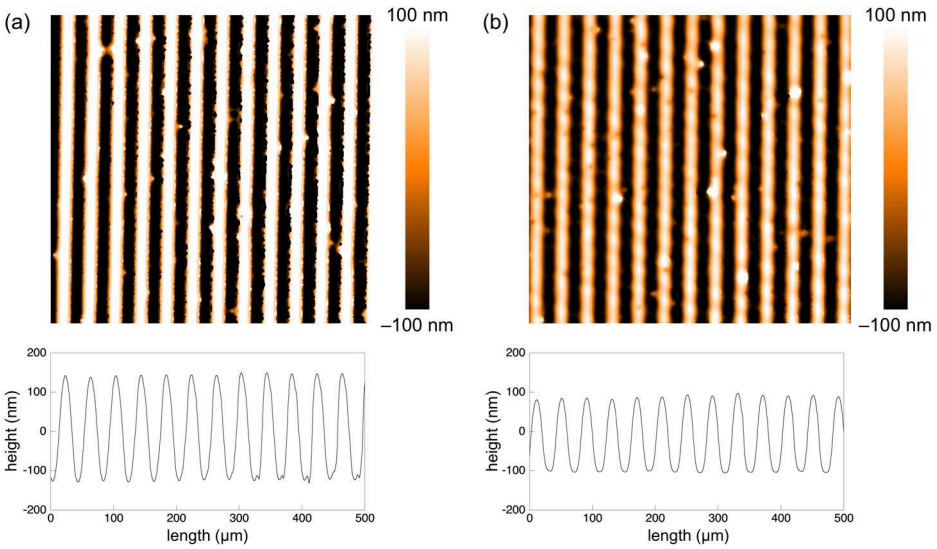

Fig. S9 WLIM topological images (top) and cross-sectional height profiles showing the height of samples (bottom) of (a) **Azb**$^{-}$-P4VP^{+} and (b) **PB**·**Azb**$^{-}$-P4VP^{+}. Patterned UV (365 nm, 5 mW/cm^2) irradiation was achieved through stripe-patterned photomasks at 140 and 130 °C for (a) **Azb**$^{-}$-P4VP^{+} and (b) **PB**·**Azb**$^{-}$-P4VP^{+}, respectively (pitch: 20 μm).

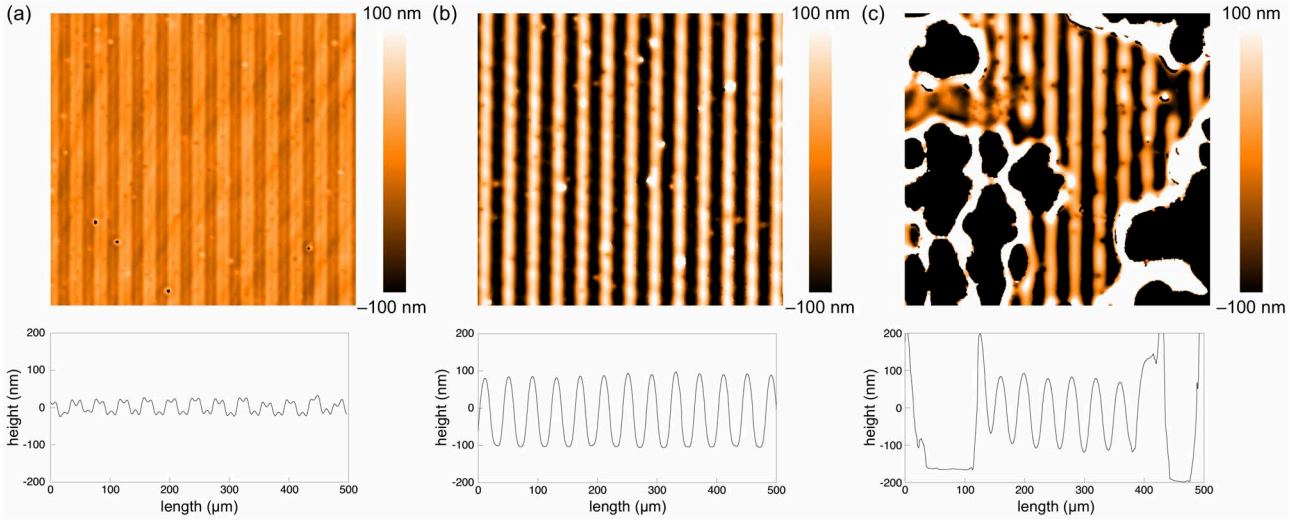

Fig. S10 WLIM topological images (top) and cross-sectional height profiles showing the height of samples (bottom) of **PB**·**Azb**$^{-}$-P4VP^{+}. Patterned UV (365 nm, 5 mW/cm^2) irradiation was achieved through stripe-patterned photomasks at (a) 120, (b) 130, and (c) 145 °C for 30 min (pitch: 20 μm). In (a,b), elevated temperature, which increased the molecular mobility and the fluidity, enabled the efficient material motion. However, in (c), the dewetting due to the aggregation occurred at the temperatures above a certain level.

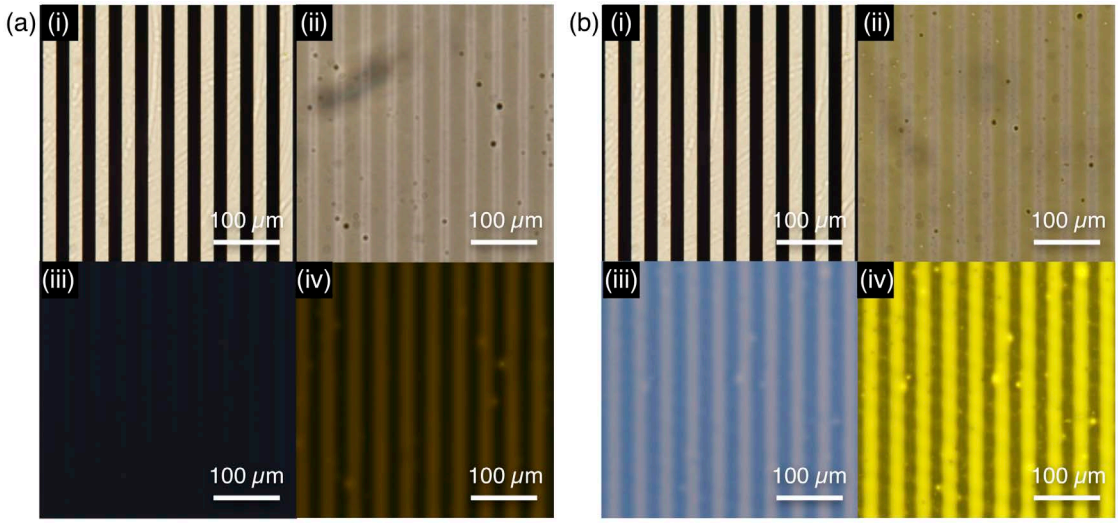

Fig. S11 Photoinduced material motion of (a) **Azb**$^{-}$-P4VP^{+} and (b) **PB**·**Azb**$^{-}$-P4VP^{+} after photoirradiation (365 nm, 5 mW/cm^2) through photomasks at 140 and 130 °C, respectively: (i) optical microscope image of stripe-patterned photomask (bright and dark areas are irradiated and shaded areas, respectively) and (ii) optical and (iii),(iv) fluorescence microscope images (excited at 365 and 436 nm for (iii) and (iv), respectively).

[S2] J. Isayama, S. Nagano and T. Seki, *Macromolecules*, 2010, **43**, 4105–4112.